Elaborated Built-In Electric Field in Mn/C$_{60}$ heterojunction Promotes Electrocatalytic Nitrogen Reduction to Ammonia

Hao Xue[ab], Kaiheng Zhao[c], Denglei Gao[d], Fangying Duan[e], Zijian Gao[f], Wenjia Yu[g],

Sha Li[*h], Menglei Yuan[*be], and Zongjing Lu[*a]

[a]Institute of Photochemistry and Photofunctional Materials, University of Shanghai for

Science and Technology, Shanghai 200093, China. E-mail: zongjinglu@usst.edu.cn

[b]Queen Mary University of London Engineering School, Northwestern Polytechnical

University, Xi'an 710129, China.

[c]Key Laboratory of Photochemistry, Institute of Chemistry, Chinese Academy of

Sciences, University of Chinese Academy of Sciences, Beijing 100190, China.

[d]School of Chemical Engineering, Shandong Institute of Petroleum and Chemical

Technology, Dongying, Shandong 257061, China.

[e]State Key Laboratory of Solidification Processing and School of Materials Science and

Engineering, Northwestern Polytechnical University, Xi'an 710072, China. E-mail:

mlyuan@nwpu.edu.cn

[f]CAS Key Laboratory of Green Process Engineering, Institute of Process Engineering,

Chinese Academy of Sciences, Beijing 100190, China.

[g]Yantai Research Institute of Harbin Engineering University, Yantai, 264006, China.

[h]Chemistry and Chemical Engineering Guangdong Laboratory, Shantou 515021, China.

E-mail: lisha@ccelab.com.cn

*Corresponding Author(s)

SI. Experimental section

1. Materials

Buckminsterfullerene [C_{60}, 99.9%], manganese carbonyl [$Mn_2(CO)_{10}$, 98%], di-sodium hydrogen phosphate dihydrate [$Na_2HPO_4 \cdot 2H_2O$, 99%], acetone [CH_3COCH_3, 99.9%], salicylic acid [$C_7H_6O_3$, $\geq$ 99.0%], sodium citrate [$C_6H_5Na_3O_7$, 98%], sodium hypochlorite (NaClO), sodium nitroferricyanide dihydrate [$C_5FeN_6Na_2O \bullet 2H_2O$, 99.0%], sodium hydroxide [NaOH, 98-100.5%], ammonium chloride [NH_4Cl, 99.5%] and Nafion membrane 211 were purchased from Sigma-Aldrich Chemical Reagent Co., Ltd. Ethanol (99.5%) were purchased from Beijing Chemical Crop. The water was purified by a Millipore system. All these reagents were used without any further purification.

2. Preparation of Mn/C_{60}

$Mn_2(CO)_{10}$ (20 mg) and C_{60} (80 mg) were put into the agate mortar and ground for 30 minutes, followed by heating to 300 °C at a heating rate of 5 °C min^{-1} under argon atmosphere. After annealing at 300 °C for 1 h, the Mn/C_{60} sample was obtained through natural cooling to room temperature.

3. Preparation of Mn

Mn NPs were synthesized to demonstrate the critical role of C_{60} in the electrocatalytic process. $Mn_2(CO)_{10}$ (40 mg) was mingled evenly and put into porcelain boat for heating treatment. Subsequently, after the same annealing and post-treatment process as in the synthesis of Mn/C_{60}, the metal Mn nanoparticles were successfully synthesized.

4. Preparation of C_{60}

The synthetic procedures for C_{60} is similar to those for Mn, C_{60} (40 mg) was mingled evenly and put into porcelain boat for heating treatment. Subsequently, proceeding the same annealing and post-treatment process as in the synthesis of Mn/C_{60}.

5. Characterization

X-ray diffraction (XRD, X'PERT PRO MPD diffractometer, Cu Kα radiation, λ=0.15418 nm, scanned range of 2-90°) was used to identify the crystal structure of all prepared catalysts. Scanning electron microscopy (SEM, JSM-7800F Prime) and transmission electron microscopy (TEM, JEM-2100F) were utilized to investigate the morphology of all samples. X-ray photoelectron spectroscopy (XPS) data were collected by using Krato, AXIS-HS monochromatized Al Kα cathode source of 75-150 W under ultrahigh vacuum. Moreover, the UV-visible adsorption spectra were recorded on a spectrophotometer (UV-2550). H NMR spectra were collected on a superconducting-magnet NMR spectrometer (Bruker AVANCE III HD 700 MHz). Besides, dimethyl sulphoxide was utilized as an internal standard to calibrate the chemical shifts in the spectra.

6. Electrochemical measurements

In order to eliminate any ammonia and other contaminants, all components of the electrochemical cell were firstly soaked in 0.05 M H_2SO_4 solution for 24 h and then washed copiously with fresh ultrapure water before NRR tests. Besides, all labware (needles, vials, pipet tips, containers, etc.) utilized in this work were also treated by 0.1 M H_2SO_4 solution and water. All electrochemical characterizations were performed using a CHI 660E workstation coupled with a three-electrode system in a single-

chamber electrolytic cell. Carbon cloth utilized in this work was purchased from CeTech (W1S1009 type) and treated with the mixture of H_2SO_4:H_2O_2 (1:3 vol.) for 12 h to remove surface impurities. To avoid excessive oxidation by oxygen and contamination with ambient ammonia or other nitrogen-containing species in air, electrodes were used either immediately after preparation or kept in vacuum before being used in electrochemical experiments. The prepared catalyst loaded on a piece of pretreated carbon cloth (1×1 cm^2) was used as the working electrode, a graphite rod and Ag/AgCl (saturated KCl electrolyte) were employed as counter electrode and reference electrode, respectively. Potential without iR-compensated were converted to RHE scale via the following equation: E (vs. RHE) = E (vs. Ag/AgCl) + 0.7736. The catalyst ink for working electrode was prepared by dispersing 2 mg of catalyst in a mixed solution of 15 μL Nafion (0.5 wt%), 250 μL acetone and 235 μL water followed by sonication for 30 minutes. Mass loading of 0.3 mg cm^{-2} was used for electrochemical study. All experiments were carried out at room temperature (25°C). To remove the impurities in the inlet gas, such as NH_3 and NO_X, the prepurification of high-purity N_2 (purity 99.999%) and Ar (purity 99.99%) by passing through a saturator filled with 0.05 M NaOH and a saturator filled with 0.05 M H_2SO_4 solution to remove any possible contaminants. Before carrying out all the electrochemical characterizations, the 0.08 M Na_2HPO_4 electrolyte solution was purged with N_2 for 30 minutes. Cyclic voltammetry (CV) test was carried out on at a scan rate of 50 mV s^{-1} ranging from -1.2264-0.7736 V (vs. RHE). Linear sweep voltammetry (LSV) was also conducted at a scan rate of 10 mV s^{-1}. Chronoamperometric test were then conducted at different potentials and pure

N_2 was continuously fed into the cathodic cell during the experiments.

7. Calculation of Faradaic efficiency (FE) and NH_3 formation rate

The FE for NRR was defined as the amount of electric charge used for producing NH_3 divided the total charge passed through the electrodes during the electrolysis. Assuming three electrons were needed to produce one NH_3 molecule, the FE was calculated according to the following equation:

$$FE = 3 \times 0.318 \times F \times C_{NH4Cl} \times V / (17 \times Q)$$

The rate of formation of NH_3 was calculated using the following equation:

$$NH_3 \text{ yield rate} = 0.318 \times C_{NH4Cl} \times V / (m_{cat} \times t)$$

Where F is Faraday constant (96485 C mol^{-1}), C_{NH4Cl} is the measured mass concentration of NH_4Cl; V is the volume of the cathodic reaction electrolyte; Q is the quantity of applied charge/electricity; t is the time for which the potential was applied; m_{cat} is the mass of catalyst loaded at the carbon cloth.

8. DFT calculations

The first-principles spin-polarized calculations were carried out using the Vienna Ab initio Simulation Package (VASP). [1, 2] The exchange-correlation energy was modeled with the Perdew-Burke-Ernzerhof (PBE) functional within the generalized gradient approximation (GGA). [3, 4] The interactions between ions and electrons were accurately described using the projector augmented wave (PAW) method. [5] A plane-wave basis set with a cutoff energy of 500 eV was employed throughout the calculations. Convergence criteria for energy and force were set to 10^{-5} eV and 0.01 eV/Å, respectively. For structural relaxation, the Brillouin zone was sampled using a $3 \times 3 \times 1$ grid based on the Monkhorst-Pack scheme. Long-range van der Waals (vdW) interactions were accounted for with Grimme's DFT-D3 dispersion correction method. A vacuum slab of over 15 Å was applied along the z-direction. The change in free

energy (ΔG) for each hydrogenation step was computed using the computational hydrogen electrode (CHE) model, [7] where ΔG for each surface was defined by the equation: $\Delta G = \Delta E + \Delta E_{ZPE} - T\Delta S + \Delta G_U + \Delta G_{pH}$. Here, ΔE was derived from DFT calculations, ΔE_{ZPE} represents the zero-point energy (ZPE) corrections, and ΔS accounts for entropy corrections. The temperature (T) was set to 298.15 K, and the pressure was set to 0.1 MPa. ΔG_U represents the contribution of the applied potential, with U being the applied electrode potential. ΔG_{pH} is the free energy correction for the H$^+$ concentration, defined as $\Delta G_{pH} = k_B T \times \ln 10 \times pH$, where kB is the Boltzmann constant and the pH value is zero. The limiting potential (U_L) for the overall elementary step was calculated by determining the potential-determining step (PDS), which exhibits the most positive Gibbs free energy change (ΔG_{max}), using the formula: $U_L = - \Delta G_{max}/e$.
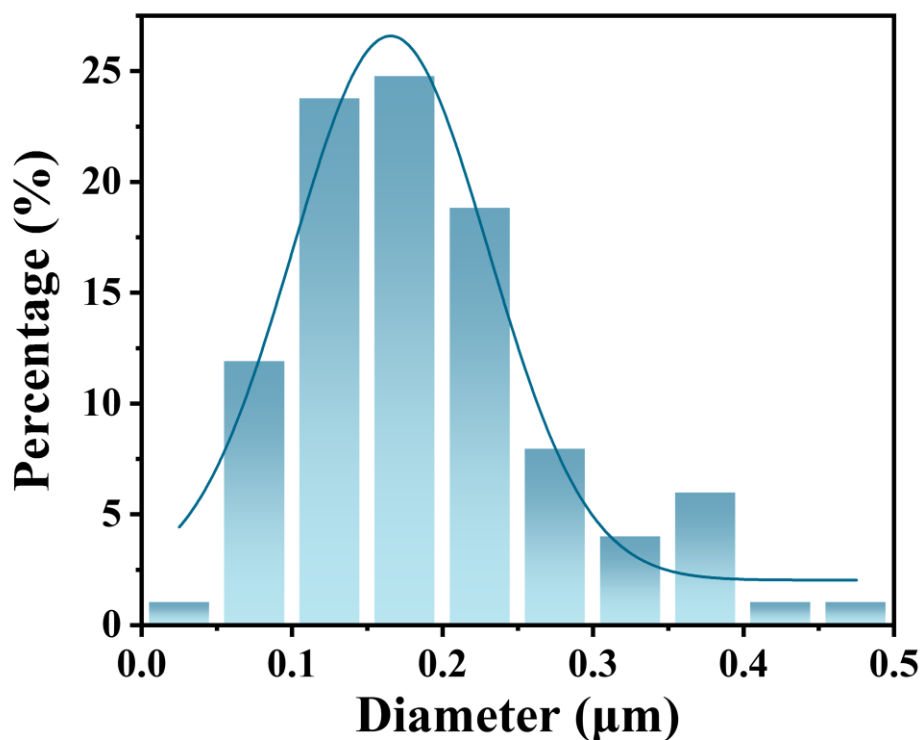
Figure S1. Average size distribution measured in SEM for 101 particles utilizing *Nano Measurer 1.2* software.

Table S1. Work function of Mn (101), C_{60} and C_{60}/Mn (101).

Slab	Work function (eV)
C_{60}	5.52
Mn(101)	3.75
C_{60}/Mn(101)	3.23
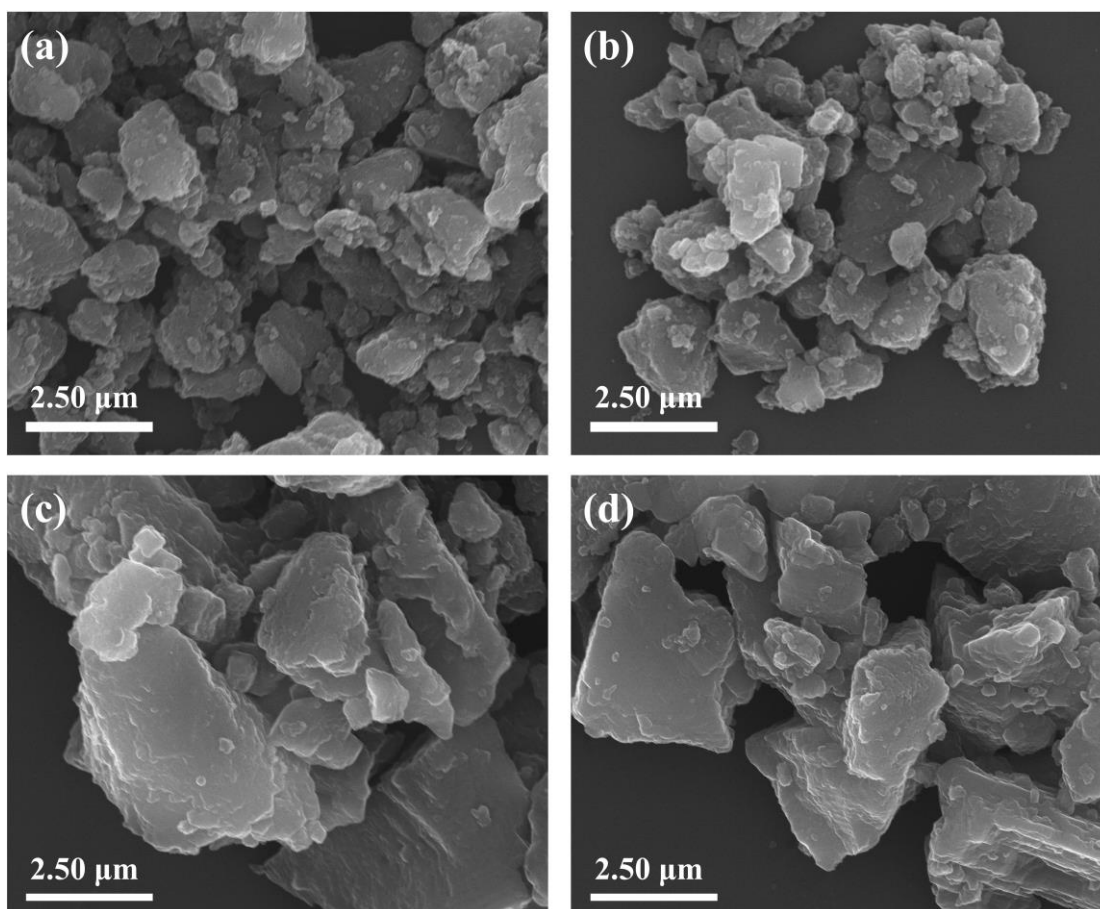
Figure S2. SEM image of synthesised (a-b) Mn/C_{60} and (c-d) C_{60}.
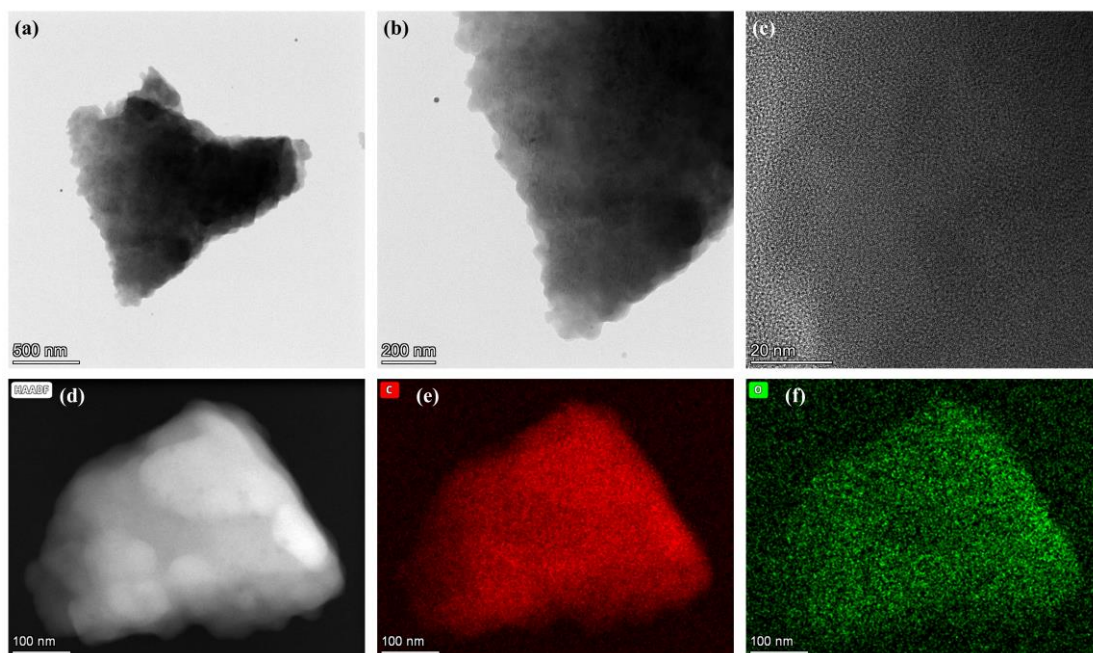
Figure S3. (a-c)The high resolution transmission electron microscopy (HRTEM) image of synthesised C_{60} and (d-f) corresponding EDS mapping images of C_{60}.
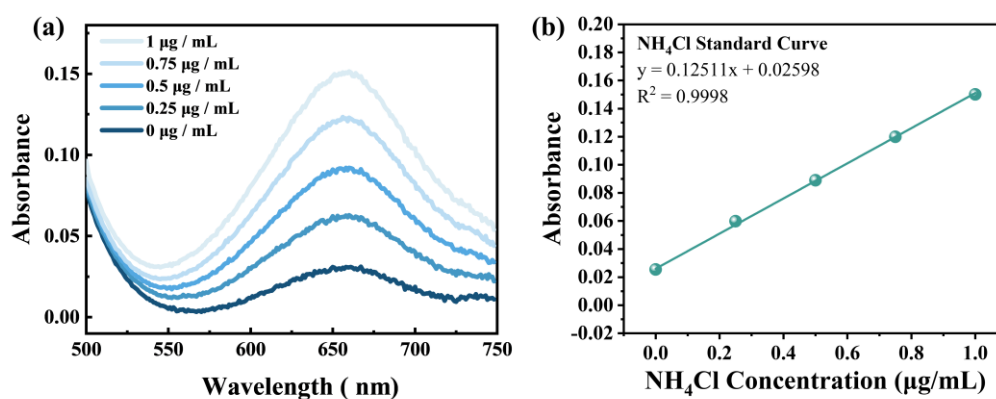
Figure S4. (a) UV-vis curves and (b) concentration-absorbance of NH_4Cl solution with a series of standard concentration (0-1 $\mu g\ mL^{-1}$) in 0.08 M Na_2HPO_4. The absorbance at 655 nm was measured by UV-vis spectrophotometer. The standard curve showed good linear relation of absorbance with NH_4Cl concentration (y=0.12511x+0.02598, R^2=0.9998).
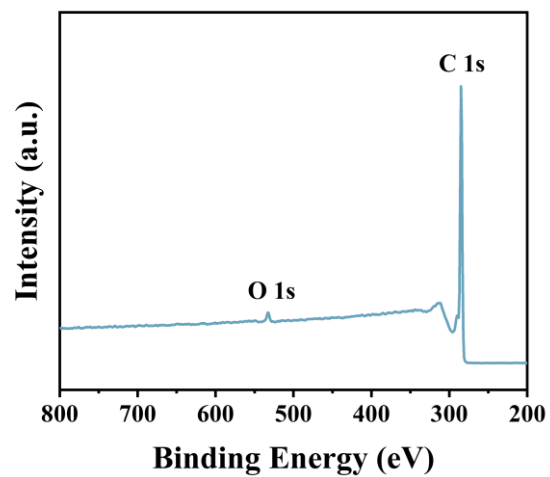
Figure S5. XPS survey spectrum of C_{60}.
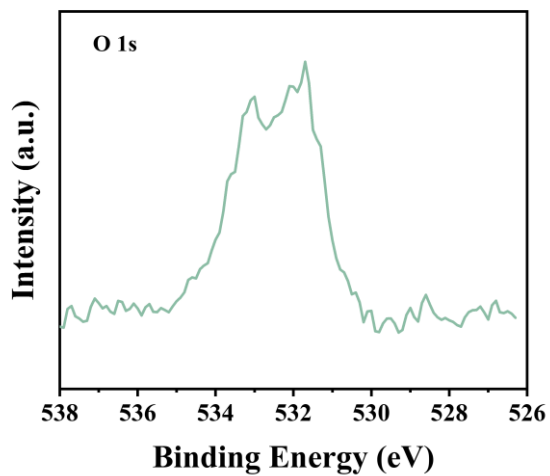
Figure S6. High-resolution XPS spectra of O 1s for C_{60}.
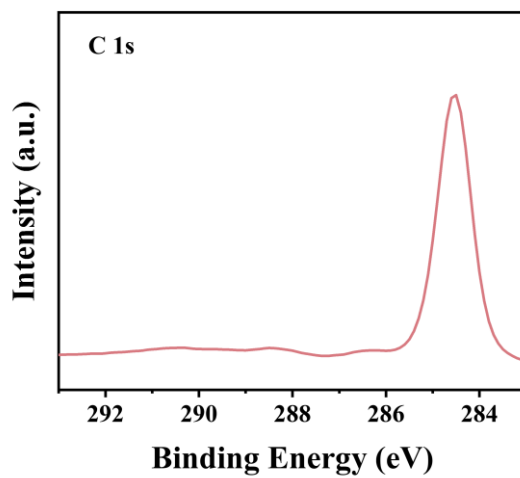
Figure S7. High-resolution XPS spectra of C 1s for C_{60}.
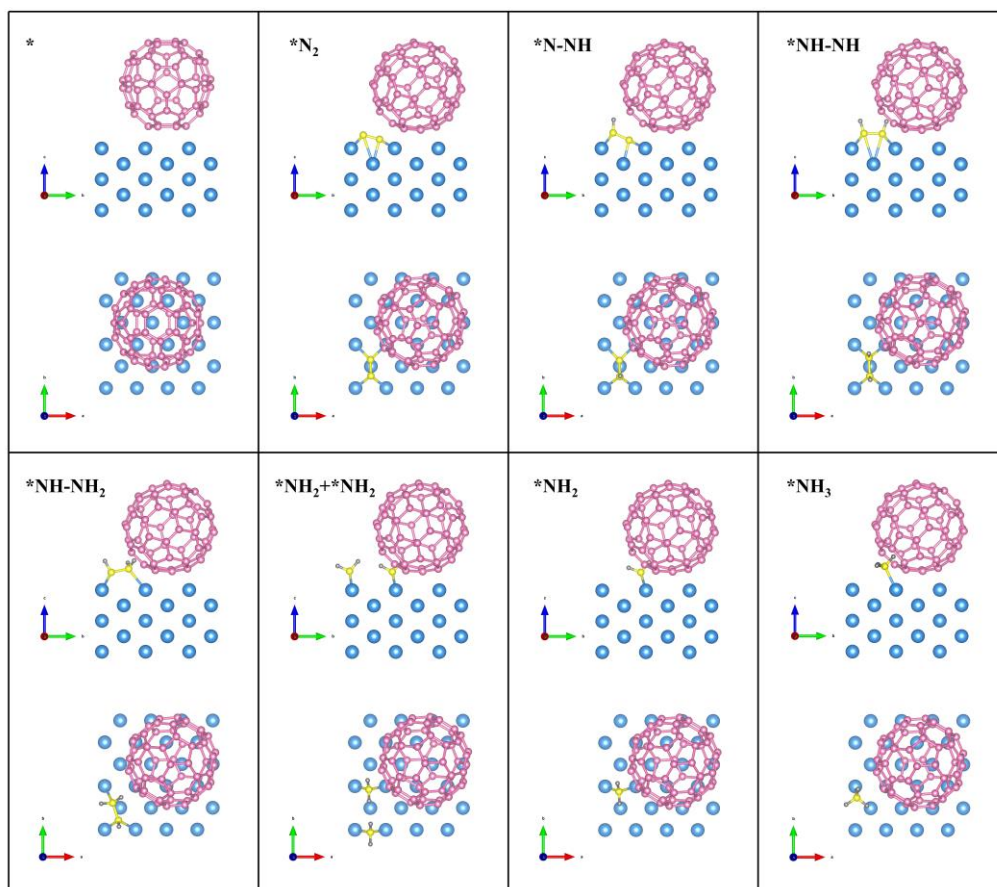
Figure S8. Adsorption configurations of different species during the NRR on Mn/C_{60}.
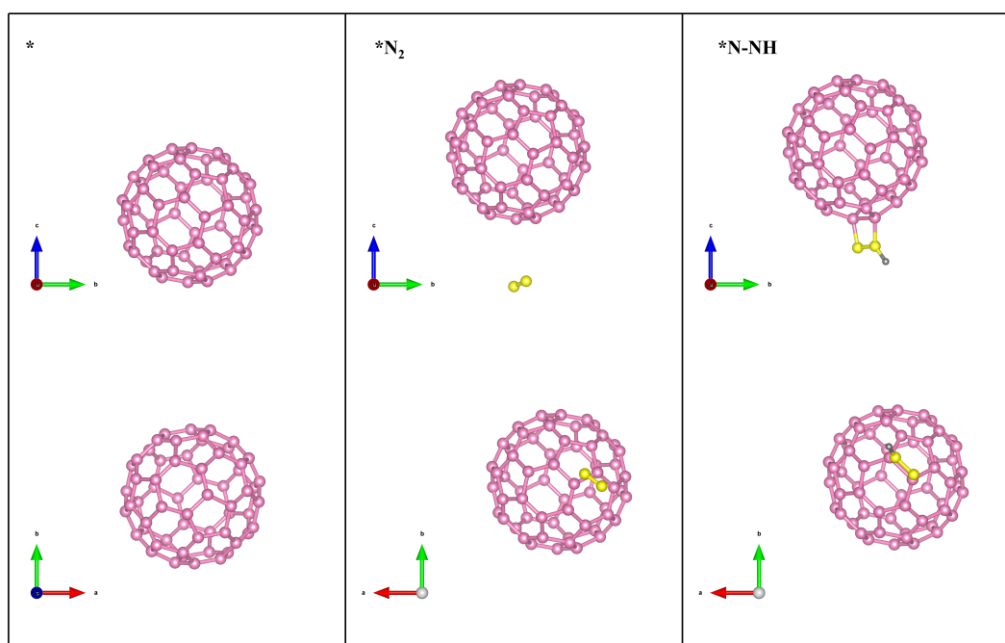
Figure S9. Adsorption configurations of different species during $N_2 \rightarrow$ *N_2H on C_{60}.
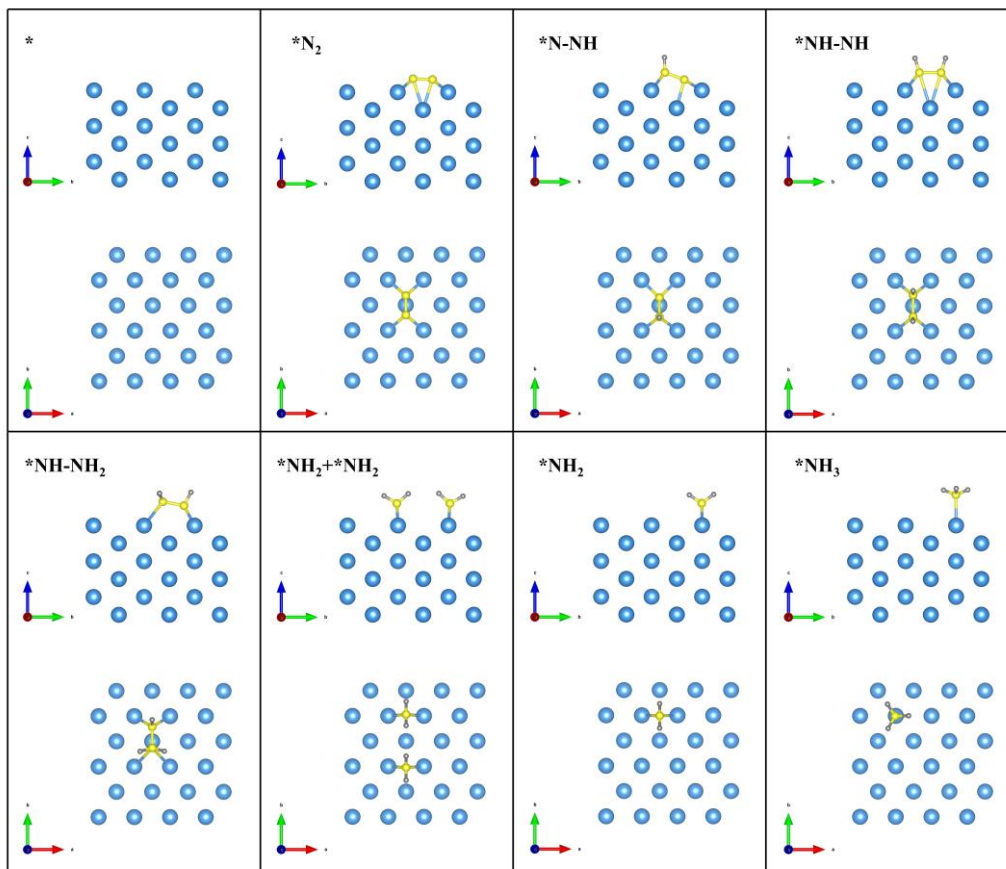
Figure S10. Adsorption configurations of different species during the NRR on Mn.

Table S2. Calculated zero-point energy (E_{ZPE}) and *TS* of different adsorption species, where * denotes the adsorption site, and 298.15 K.

Adsorption species	E_{ZPE} (eV)	*TS* (eV)
*N≡*N	0.19	0.14
*N≡N	0.21	0.13
*N-*NH	0.47	0.19
*NH-*NH	0.82	0.19
*NH$_2$-*N	0.83	0.12
*NH-*NH$_2$	1.14	0.18
*NH$_2$+*NH$_2$	1.25	0.25
*NH$_2$	0.63	0.14
*NH$_3$	1.02	0.16
*H	0.15	0.01

Table S3. Energies of N_2, H_2, NH_3 adopted in this work where E_{DFT} stands for the energy obtained from DFT calculations. For the gas molecules, their E_{ZPE} and S values (gas phase H_2, N_2, NH_3 at T = 298.15 K, P = 1 bar) are from the NIST database. (https://doi.org/10.18434/T4D303)

Species	E_{DFT} (eV)	E_{ZPE} (eV)	TS (eV)	G (eV)
H_2	-6.77	0.27	0.40	-6.90
N_2	-16.63	0.15	0.60	-17.08
NH_3	-19.54	0.91	0.60	-19.23

Table S4. Comparison of the electrocatalytic activity of Mn/C_{60} to produce NH_3 through NRR with previously reported NRR electrocatalysts.

Catalyst	NH_3 yield rate ($\mu g\ h^{-1}\ mg^{-1}$)	Faradaic efficiency (%)	Reference
Mn/C_{60}	14.52	42.18	This work
Pd/C	4.5	8.2	8
V_2O_3/C	12.3	7.28	9
$C-TiO_2$	16.22	1.84	10
Mn_3O_4 Nanocube	11.6	3	11
$F-SnO_2/CC$	19.3	8.6	12
SnO_2/CC	4.03	2.17	13
NPC	27.2	1.42	14
Nb_2O_5 nanofiber	43.6	9.26	15
$Au-Bi_2Te_3$ Nanosheets	32.73	20.39	16
WO_x/NPC	46.8	10.2	17
$PC/Sb/SbPO_4$	23	34	18

References

1. G. Kresse and J. Furthmüller, *Phys. Rev. B: Condens. Matter Mater. Phys.*, 1996, **54**, 11169-11186.

2. G. Kresse and J. Furthmuller, *Comput. Mater. Sci.*, 1996, **6**, 15-50.

3. J. P. Perdew, J. A. Chevary, S. H. Vosko, K. A. Jackson, M. R. Pederson, D. J. Singh and C. Fiolhais, *Phys. Rev. B.*, 1992, **46**, 6671.

4. J. P. Perdew and Y. Wang, Phys. Rev. B, *Condens. Matter.*, 1992, **45**, 13244-13249.

5. G. Kresse and D. Joubert, *Phys. Rev. B.*, 1999, **59**, 1758-1775.

6. S. Grimme, J. Antony, S. Ehrlich and H. Krieg, *J. Chem. Phys.*, 2010, **132**, 154104.

7. J. K. Norskov, J. Rossmeisl, A. Logadottir, L. Lindqvist, J. R. Kitchin, T. Bligaard and H. Jonsson, *J. Phys. Chem. B*, 2004, **108**, 17886-17892.

8. J. Wang, L. Yu, L. Hu, G. Chen, H. Xin and X. Feng, *Nat. Commun.*, 2018, **9**, 1795.

9. R. Zhang, J. Han, B. Zheng, X. Shi, A. M. Asiri and X. Sun, *Inorg. Chem. Front.*, 2019, **6**, 391-395.

10. K. Jia, Y. Wang, Q. Pan, B. Zhong, Y. Luo, G. Cui, X. Guo and X. Sun, *Nanoscale Adv.*, 2019, **1**, 961-964.

11. X. Wu, L. Xia, Y. Wang, W. Lu, Q. Liu, X. Shi and X. Sun, *Small*, 2018, **14**, 1803111.

12. K. Chu, Y.-p. Liu, Y.-b. Li, H. Zhang and Y. Tian, *J. Mater. Chem. A*, 2019, **7**, 4389-4394.

13. L. Zhang, X. Ren, Y. Luo, X. Shi, A. M. Asiri, T. Li and X. Sun, *Chem. Commun.*, 2018, **54**, 12966-12969.

14. Y. Liu, Y. Su, X. Quan, X. Fan, S. Chen, H. Yu, H. Zhao, Y. Zhang and J. Zhao, *ACS Catal.*, 2018, **8**, 1186-1191.

15. J. Han, Z. Liu, Y. Ma, G. Cui, F. Xie, F. Wang, Y. Wu, S. Gao, Y. Xu and X. Sun, *Nano Energy*, 2018, **52**, 264-270.

16.   M. Liu, S. Yin, T. Ren, Y. Xu, Z. Wang, X. Li, L. Wang and H. Wang, *ACS Appl. Mater. Interfaces*, 2021, **13**, 47458-47464.

17.   Z. Lu, H. Wang, Y. Tao, S. Zhu, W. Hao, X. Liu, Y. Min and J. Fan, *Nanoscale*, 2023, **15**, 14847-14857.

18.   X. Liu, H. Jang, P. Li, J. Wang, Q. Qin, M. G. Kim, G. Li and J. Cho, *Angew. Chem., Int. Ed.*, 2019, **58**, 13329-13334.